Dynamics of small, spherical particles in vortical and stagnation point flow fields

N. Raju and E. Meiburg[a)]
Department of Aerospace Engineering, University of Southern California, Los Angeles, California 90089-1191

(Received 10 July 1996; accepted 9 October 1996)

The transport in vortical and stagnation point flow fields is analyzed for particles across the entire range of density ratios, based on the Maxey–Riley equation [Phys. Fluids **26**, 883 (1983)] without history effects. For these elementary flow fields, the governing equations simplify substantially, so that analytical progress can be made towards quantifying ejection/entrapment trends and accumulation behavior. For a solid body vortex, the analysis shows that optimal ejection or entrapment occurs for all density ratios, as the difference between inward and outward forces reaches a maximum for intermediate values of the Stokes number. The optimal Stokes number value is provided as a function of the density ratio. Gravity is shown to shift accumulation regions, without affecting the entrapment or ejection rates. For a point vortex flow, the existence of up to three different regimes is demonstrated, which are characterized by different force balances and ejection rates. For this flow, optimal accumulation is demonstrated for intermediate Stokes numbers. The stagnation point flow gives rise to optimal accumulation for heavy particles, whereas light particles do not exhibit optimal behavior. The analysis furthermore indicates that nonvanishing density ratios give rise to a finite Stokes number regime in which the particle motion is oscillatory. Above and below this regime, the motion is overdamped. © *1997 American Institute of Physics.* [S1070-6631(97)00202-X]

I. INTRODUCTION

The transport of heavy particles, drops, and bubbles in a variety of flow fields has received wide attention in recent years, owing to its importance in both engineering and natural flows. Technological applications concern, for example, pollution reduction and efficiency enhancement through improved mixing of the fuel droplets in an internal combustion engine. Similarly, control over the droplet dynamics in the final stages of large turbines can avoid impact erosion of the blades. A different, but related issue arises in the recently developed experimental technique of particle image velocimetry (PIV). Here, the fluid motion is to be tracked by either droplets or solid particles. An obvious question concerns the tracking ability of particles whose density or initial velocity does not quite match the fluid properties.

Over the last decade, both experimental and computational investigations have addressed the issue of the dispersion of heavy particles and bubbles, with particular emphasis on free shear flows, such as mixing layers, jets, and wakes. Numerous studies have demonstrated the strong influence of the coherent vortical flow structures. These are observed to preferentially disperse heavy particles whose aerodynamic response time is of the same order as the characteristic flow time scale, i.e., particles whose Stokes number St is near unity. For these particles of intermediate size, both numerical[1–5] and experimental[6–9] investigations demonstrate the ejection of the particles from the vortex centers, as well as their accumulation in the outer regions of the vortices and in the neighborhood of stagnation points. The formation of streaks of high particle concentrations plays an important role in the overall dynamics of the dispersion process. A recent review of the relevant work is given by Crowe *et al.*[10] For bubbly flows, numerical simulations have demonstrated the preferential entrapment[11,12] of bubbles of intermediate St, along with the modification of the flow by the bubbles.[13] In contrast to the behavior of heavy particles, the bubble concentration is found to decrease in the outer regions of the vortices.

From the above experimental and computational investigations, it becomes clear that the global features of bubble and particle dispersion are dominated by their dynamics in three distinctly different regions of the flow field: the viscously dominated vortex core, the outer region of the vortices, and the stagnation zones. Several investigations have addressed the dynamics of particles and bubbles in idealized representations of these flows.[3,4,11,14–17] However, these studies were mostly limited to situations in which the ratio between particle and fluid density is either zero or infinity. The present investigation aims at analyzing in detail the dynamics of particles across the entire spectrum of density ratios and St values, and at elucidating the governing force balances in the different parameter regimes. A combination of analytical and numerical approaches will be employed towards this end. The vortex core region will be approximated as a solid body vortex, while the outer vortical region can be analyzed on the basis of a point vortex model. Finally, the stagnation zone will be modeled in a linear fashion as well. For all of these model flows, particular attention will be paid to situations of interest in PIV applications, namely nearly neutrally buoyant particles, and particles with mismatched initial velocities.

[a)]Corresponding author: Department of Aerospace Engineering, University of Southern California, Los Angeles, California 90089-1191. Phone: 213-740-5376; Fax: 213-740-7774.

Downloaded¬22¬May¬2004¬to¬128.111.70.70.¬Redistribution¬subject¬to¬AIP¬license¬or¬copyright,¬see¬http://pof.aip.org/pof/copyright.jsp

The equations governing the particle motion are outlined in section II. In section III we address the core region, while in section IV we focus on the point vortex model. Subsequently, the stagnation point flow is analyzed in section V, while in section VI we summarize the results and present several conclusions.

II. EQUATIONS GOVERNING THE PARTICLE MOTION

We consider the dilute limit, in which there is only one-way coupling from the fluid to the particle. The concentration of the particles is assumed to be small enough so that both the particle–particle and particle–fluid interactions are negligible. The resulting equation of motion for the particles is then obtained by neglecting the the Faxen correction terms in the relationship first derived by Maxey and Riley[18]

$$V\rho_p\frac{d\mathbf{v}_p}{dt}=3\pi\phi\mu[\mathbf{u}(\mathbf{x},t)|_{\mathbf{x}=\mathbf{x}_p(t)}-\mathbf{v}_p(t)]+V(\rho_p-\rho_f)\mathbf{g}+V\rho_f\frac{D\mathbf{u}}{Dt}\bigg|_{\mathbf{x}=\mathbf{x}_p(t)}+\frac{1}{2}V\rho_f\frac{d}{dt}[\mathbf{u}(\mathbf{x},t)|_{\mathbf{x}=\mathbf{x}_p(t)}-\mathbf{v}_p(t)]-\frac{3}{2}\pi\phi^2\mu\times\int_0^t\left\{\frac{d/d\tau[\mathbf{v}_p(\tau)-\mathbf{u}(\mathbf{x},t)|_{\mathbf{x}=\mathbf{x}_p(t)}]}{[\pi\mu(t-\tau)/\rho_f]^{1/2}}\right\}d\tau. \tag{1}$$

Here $\mathbf{v_p}$ and $\mathbf{u}$ denote the particle and fluid velocity, respectively. While ρ_f, and μ are the density and dynamical viscosity of the surrounding fluid, the symbols ϕ, V, and $\mathbf{x}_p(t)$ represent the diameter, volume, and position of the particle, respectively. The total derivative with respect to the particle is denoted by d/dt, while that with respect to the fluid is given by D/Dt. The right hand side of this equation represents the forces acting on the particle. In order, these are the Stokes drag, gravity, a pressure gradient force accounting for the acceleration of the displaced fluid and the virtual mass, and the Basset history term. Manton[14] and Auton[19] argue that $D\mathbf{u}/Dt$ should be used in the added mass term instead of $d\mathbf{u}/dt$. Ruetsch and Meiburg[11] show that, for example, in a solid body vortex the particle trajectory is nearly independent of the form of the added mass term. Consequently, in the following we will employ the respective form of the added mass term that keeps the mathematics simplest. Equation (1) describes the particle motion accurately provided

$$\frac{\phi}{\gamma}\ll 1,\qquad Re_p=\frac{\phi\overline{U}}{\nu}\ll 1,\qquad \frac{\phi^2 U}{\gamma\nu}\ll 1, \tag{2}$$

where $\overline{U}$ is the slip velocity between the particle and the surrounding fluid, γ and U denote the characteristic length and velocity scales of fluid motion, respectively, and ν is the kinematic viscosity.

Recently, the Basset history term has been examined more closely by several research groups.[20–29] Through a combination of analytical and computational investigations, they find that the history term decays initially as $t^{-1/2}$ and later as t^{-2}. As a result, history effects are less important than originally thought, so that within the present investigation we neglect them entirely. The forces driving the particle motion in our model are the particle inertia, the pressure gradient, the added mass term, and the viscous Stokes drag. In some situations, we will analyze the effect of gravity as well. It should be mentioned that all of the above forces were included in Maxey's[30] study of particle dynamics in cellular flows as well.

III. VORTEX CORE REGION

As a first step, we analyze the motion of a particle in the core region of a vortex, which we approximate as a solid body vortex with the velocity components,

$$u_x=-\frac{\Omega_0}{2}y, \tag{3}$$

$$u_y=+\frac{\Omega_0}{2}x, \tag{4}$$

where Ω_0 is the vorticity of the solid body vortex. The problem exhibits a characteristic time scale in the form of the eddy turnover time $T=1/\Omega_0$, whereas length or velocity scales are absent. Consequently, after neglecting the Basset history and gravity terms, the dimensionless version of Eq. (1) takes the form

$$\left(1+\frac{1}{2}\delta\right)\ddot{x}=-\frac{\delta}{4}x-\frac{1}{4}\delta\dot{y}+\frac{1}{St}\left(-\frac{y}{2}-\dot{x}\right), \tag{5}$$

$$\left(1+\frac{1}{2}\delta\right)\ddot{y}=-\frac{\delta}{4}y+\frac{1}{4}\delta\dot{x}+\frac{1}{St}\left(\frac{x}{2}-\dot{y}\right), \tag{6}$$

$$\delta=\rho_f/\rho_p,\qquad St=\frac{\rho_p\phi^2}{18\mu}\Omega_0, \tag{7}$$

where δ is the density ratio and St denotes the particle Stokes number. In the present context, St can be interpreted as the ratio of the particle's aerodynamic response time and the characteristic time scale T of the fluid motion. A larger particle density results in a lower density ratio and an increased Stokes number. On the other hand, a change in size affects St only. In the following, we will refer to light particles if $\delta>1$, and to heavy particles if $\delta<1$. For the limit of very heavy particles ($\delta\to 0$), Raju and Meiburg[4] discuss the ejection trends in a solid body vortex under the effects of particle inertia and Stokes drag only. They present a quantitative scaling argument that explains the preferential dispersion of particles with St near unity in free shear flows. Ruetsch and Meiburg,[11] on the other hand, address the bubble limit ($\delta\to\infty$), which can most conveniently be treated by redefining the Stokes number as

$$St'=St\,\delta=\frac{\rho_f\phi^2}{18\mu}\Omega_0. \tag{8}$$

This definition reflects the importance of the added mass in the bubble limit. In the present investigation we address the entire range between the heavy particle and the bubble limits.

The current problem represents a fourth order linear dynamical system. In order to solve the governing equations,

Downloaded¬22¬May¬2004¬to¬128.111.70.70.¬Redistribution¬subject¬to¬AIP¬license¬or¬copyright,¬see¬http://pof.aip.org/pof/copyright.jsp

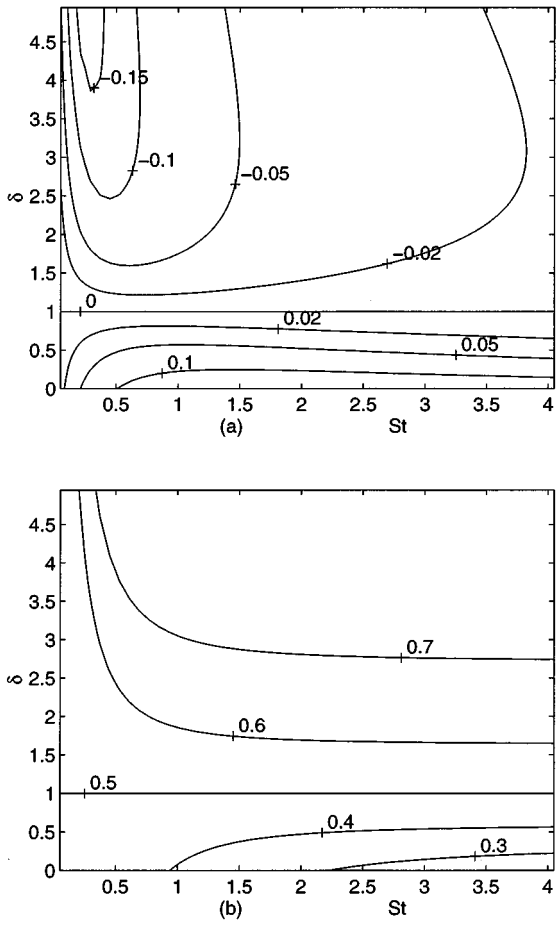

FIG. 1. Particle motion in a solid body vortex: Contour plots of (a) the real, and (b) the imaginary parts of the eigenvalue with the largest real part. The real part represents the long time ejection and entrapment rates, which are optimized for intermediate values of $St(\delta)$. The imaginary part expresses the long time rotation rate. While light particles rotate faster than the surrounding fluid, heavy particles rotate more slowly.

first the roots of a quartic polynomial for the eigenvalues need to be obtained. By treating the problem in the complex variable $z=x+iy$, it is reduced to the quadratic equation in z,

$$(1+\delta/2)\ddot{z}+\left(\frac{1}{St}-i\frac{\delta}{4}\right)\dot{z}+\left(\frac{\delta}{4}-i\frac{1}{2St}\right)z=0, \tag{9}$$

which has solutions of the form

$$z=x+iy=c_1e^{\lambda_1 t}+c_2e^{\lambda_2 t}, \tag{10}$$

$$\lambda_{1,2}=(-b\pm\sqrt{b^2-4ac})/(2a), \qquad a=1+\delta/2, \tag{11}$$

$$b=1/St-i\,\delta/4, \qquad c=\delta/4-i/(2St). \tag{12}$$

It is clear from Eq. (10) that particles either approach the origin ($z=0$) or asymptotically recede away to infinity, depending on whether the sign of the largest real part of the eigenvalues, $Re(\lambda_1)$, is negative or positive, respectively. For heavy particles, $Re(\lambda_1)$ is always positive, while $Re(\lambda_2)$ is negative. For light particles, the real parts of both eigenvalues are negative, with $Re(\lambda_1)>Re(\lambda_2)$. Consequently, heavy particles are ejected from the vortex core, whereas light particles asymptotically approach the vortex

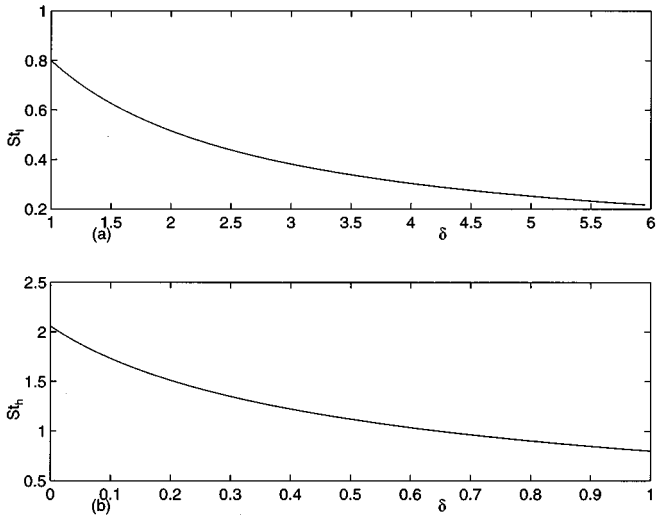

FIG. 2. Stokes number for which optimal entrapment/ejection trends are observed as a function of the density ratio δ. (a) St_l for light particles and (b) St_h for heavy particles.

center. For the sake of convenience, we let λ_r and λ_i denote the real and imaginary parts of the largest eigenvalue λ_1, respectively. The second term in Eq. (10) represents an initial transient, which persists for longer times as St is increased.

Figure 1(a) represents a contour plot of λ_r in the St,δ-plane. The negative values for $\delta>1$ indicate that light particles, in agreement with the above discussion, are entrapped in the core, so that they approach the vortex center asymptotically. For every $\delta>1$, there is an optimal Stokes number St_l, for which the entrapment rate is maximized. The value of St_l decreases as δ is increased; cf. Fig. 2(a). In the limit as $\delta\to\infty$, the problem should be treated with the modified Stokes number St'. Here the entrapment rate becomes optimal when $St'=0.74$, in agreement with Ruetsch and Meiburg.[11]

Heavy particles, on the other hand, are ejected, as is evident from the positive values of λ_r [Fig. 1(a)]. For a given value of St, the ejection rate decreases with increasing δ. However, for a given value of δ the ejection rate is maximized for an intermediate value of the Stokes number, St_h. St_h increases with decreasing δ [Fig. 2(b)]. The optimal ejection of intermediate-sized particles (as expressed by St_h) is in agreement with both experimental and computational investigations of particle dispersion in mixing layers, jets, and wakes, as discussed in the Introduction.

Because the balance of forces responsible for the observed entrapment/ejection trends is intricately related to the rotation rates of the particles, we first analyze the trends in the rotation rates, before continuing the discussion on entrapment/ejection. λ_i corresponds to the circular frequency or rotation rate, $\dot{\theta}$ of the particle, after the initial transient has decayed. After this decay, the particle trajectory can be visualized as a spiral centered about the origin. Heavy particles spiral outward, while light ones spiral inward. Along this spiral, the rotation rate, plotted in Fig 1(b), is a constant expressed by λ_i. The figure shows that the rotation rate of

Downloaded¬22¬May¬2004¬to¬128.111.70.70.¬Redistribution¬subject¬to¬AIP¬license¬or¬copyright,¬see¬http://pof.aip.org/pof/copyright.jsp

heavy particles is less than the constant value of one-half for the fluid, and that, for a given δ, it decreases with increasing St. This behavior is mostly due to the drag force, which accelerates the heavy particle as it reaches larger radii. As St is increased, the drag force and hence the particle acceleration become proportionally weaker, thereby resulting in lower rotation rates.

For light particles, the converse of the above effects hold, i.e., light particles rotate faster than the local fluid, and for a given δ, their rotation rate increases with increasing St. Now the Stokes drag decelerates the particle's azimuthal motion. However, since the drag force per mass decreases wih increasing St, the rotation rate of light particles increases with increasing St. The increase (decrease) in the rotation rate for light (heavy) particles with increasing St can be demonstrated by means of a brief mathematical analysis as well; cf. the Appendix.

We now return to the entrapment/ejection trends discussed earlier. The force balance responsible for entrapment/ejection can be understood more easily by casting the equations of motion in polar coordinates. We obtain

$$(1+\delta/2)\frac{\ddot{r}}{r} = -\delta/4 - \delta\dot{\theta}/4 - \frac{1}{St}\frac{\dot{r}}{r} + (1+\delta/2)\dot{\theta}^2, \tag{13}$$

$$(1+\delta/2)(r\ddot{\theta} + 2\dot{r}\dot{\theta}) = \frac{\delta\dot{r}}{4} + \frac{1}{St}(r/2 - r\dot{\theta}). \tag{14}$$

These equations are nonlinear, and hence difficult to solve analytically. However, further simplifications are possible if we limit ourselves to the long time behavior. Per our earlier discussion, the rotation rate becomes a constant after the initial transients have died out. Its value can be obtained as a function of the ejection/entrapment rate and St by setting $\ddot{\theta}=0$ in Eq. (14),

$$\dot{\theta} = \frac{\frac{1}{2} + (\delta/4)(\dot{r}/r)\,St}{1+(2+\delta)St\,(\dot{r}/r)}. \tag{15}$$

With $\dot{r}/r$ representing the long term ejection/entrapment rate λ_r, this yields

$$\dot{\theta} = \frac{\frac{1}{2} + (\delta/4)\,\lambda_r St}{1+(2+\delta)St\lambda_r}. \tag{16}$$

We now consider the different forces acting along the radial direction. The last term in Eq. (13), which combines the rotation rate dependent component of the inertia (centrifugal force) with the pressure gradient and added mass forces, always points outward. With the vortex center corresponding to a pressure minimum, the pressure gradient force is directed inward, as reflected by the sign of the first term on the rhs of Eq. (13). The added mass, on the other hand, contributes to several forces: (1) it increases the inertia ($\delta/2$ term on the lhs), (ii) it increases the centrifugal force, and (iii) it adds an inward force (second term on the rhs). The Stokes drag, may it be inward or outward, always opposes motion.

Let us now analyze how the different radial forces [rhs of Eq. (13)] acting on a heavy particle vary with St for a given δ. The first three terms on the rhs of Eq. (13) oppose the outward motion of the particle, while the fourth term causes the outward motion. When St is increased, the outward centrifugal force decreases because the rotation rate decreases, as discussed earlier. The sum of the three inward forces can also be shown to decrease if St is increased. The first inward force from the rhs of Eq. (13) does not depend on St. The second inward force decreases in magnitude with increasing St, because the rotation rate decreases. The third inward force decreases as well with increasing St, as can be seen from the following argument. Recall that the ratio $\dot{r}/r$, present in the numerator, is the ejection rate λ_r. The third term can then be expressed as λ_r/St. Contour plots of this ratio, shown in Fig. 3, reveal that for a given $\delta<1$, this ratio decreases as St is increased. Thus both the outward and the inward forces decrease with increasing St. However, it is the *difference* between the inward and the outward forces that causes the particles to move. We therefore analyze how this difference varies as a function of St for a given δ. From Fig. 4, which depicts this difference as contours in the St,δ-plane, we can conclude that it is maximized at intermediate values of St, thereby causing the optimal ejection of heavy particles.

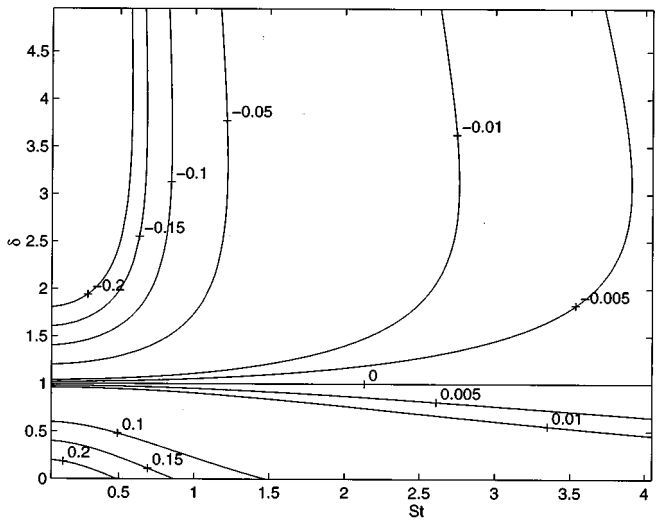

FIG. 3. Contour plots of the drag force λ_r/St. The sign of the contour levels indicates the direction of the force. For a given value of δ, the magnitude of the drag increases for both heave ($\delta<1$) and light ($\delta>1$) particles if St is increased.

For light particles, the inward forces are due to the first two terms on the rhs of Eq. (13), whereas the outward forces are due to the last two terms. The sum of the inward forces grows with increasing St, because of an increase in the rotation rate. The third term, expressing the Stokes drag force, now points outward. This force decreases with increasing St (Fig. 3). The fourth term, a combination of centrifugal, pressure gradient, and added mass forces, which increases with St. Via graphical inspection of a contour plot, one finds that the sum of these two outward forces increases as well. Thus both the inward and the outward forces increase with St. However, as demonstrated in Fig. 4, their difference is maximized for intermediate values of St, thereby causing optimal entrapment.

Downloaded¬22¬May¬2004¬to¬128.111.70.70.¬Redistribution¬subject¬to¬AIP¬license¬or¬copyright,¬see¬http://pof.aip.org/pof/copyright.jsp

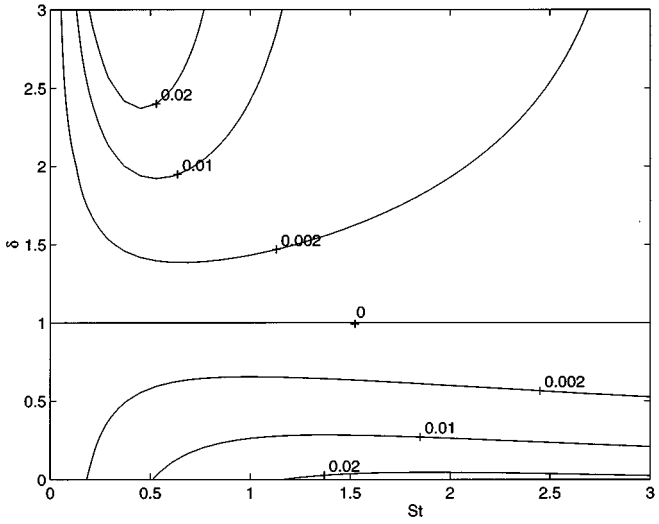

FIG. 4. The *difference* between the outward and inward radial forces plotted as contours in the St, δ-plane. As St is increased, this difference is maximized for intermediate values of St for both heavy ($\delta<1$) and light ($\delta>1$) particles.

If $\delta=1$ and the particle velocity is equal to that of the surrounding fluid, the radial force acting on it is identically equal to zero according to Eq. (13). As a result, neutrally buoyant particles follow the fluid exactly, provided their initial velocity matches that of the fluid. If, on the other hand, the initial velocity of the particle differs from that of the fluid, the particle trajectory can be analyzed using Eq. (10). When $\delta=1$, the eigenvalues can be expressed as

$$\lambda_1 = 0 - i\,\tfrac{1}{2},$$

$$\lambda_2 = -\frac{2}{3St} + i\,\frac{1}{3}.$$

The solution then takes the form

$$z = c_1\,\exp(\lambda_1 t) + c_2\,\exp(\lambda_2 t).$$

The second term vanishes as $t\to\infty$. By evaluating c_1, we find that the particle asymptotically deviates to another radius located at a distance equal to the initial velocity difference times the square of St. At this new radius, it will track the fluid motion accurately. It should be pointed out, however, that the above argument neglects history effects, which, under some circumstances, might modify the short time consequences of velocity mismatches.

A common situation arises when particles with a density slightly different from that of the fluid are used to track the fluid motion, for example due to density variations in the flow field. Hence it is of interest to analyze the effect of small density variations on the particles' tracking capability, i.e., situations with $\delta=1+\epsilon$. From the above it follows that particles are ejected if $\epsilon<0$ and entrapped if $\epsilon>0$. The ejection/entrapment rate can be obtained from Eq. (10) by performing a small ϵ expansion of the eigenvalue λ_1

$$\lambda_1 = \frac{-[1/St + i(\delta/4)] + \sqrt{1/St^2 - 9\delta^2/16 - \delta + i(2/St + \delta/2St)}}{2+\delta}. \tag{17}$$

The real part is given by

$$\lambda_r = \frac{-(1/St) + \sqrt{(d+\sqrt{d^2+f^2})/2}}{2(1+\delta/2)}, \tag{18}$$

$$d = \frac{1}{St^2} - \frac{9\delta^2}{16} - \delta, \tag{19}$$

$$f = \frac{\delta}{2St} + \frac{2}{St}. \tag{20}$$

When $\delta=1$, one can show that

$$\frac{d\lambda_r}{d\delta} = -\frac{St}{4(1+25St^2/16)}, \tag{21}$$

so that

$$\lambda_r = -\frac{St\epsilon}{4(1+25St^2/16)}. \tag{22}$$

Hence, the particle tracks the motion of the fluid accurately only for $t \ll 4(1+25St^2/16)/(|\epsilon|St)$, provided that history effects are negligible. Therefore, the smaller the particle Stokes number, the larger is the time for which the particle tracks the fluid accurately. From the definition of the Stokes number, we can infer that the tracking accuracy can be improved by increasing the viscosity or by decreasing the diameter. The accuracy also improves if the vorticity Ω_0 is reduced.

A. Effect of gravity

When gravity acts in the $-y$ direction, a characteristic length scale emerges, which is related to the terminal velocity v_t of the particle in still fluid,

$$v_t = (\rho_f - \rho_p) g \frac{\phi^2}{18\mu}, \tag{23}$$

and the eddy turnover time $1/\Omega_0$. After making the governing equations dimensionless with this length scale, they take the form

$$\left(1+\frac{1}{2}\delta\right)\ddot{x} = -\frac{\delta}{4}x - \frac{1}{4}\delta\dot{y} + \frac{1}{St}\left(-\frac{y}{2} - \dot{x}\right), \tag{24}$$

$$\left(1+\frac{1}{2}\delta\right)\ddot{y} = -\frac{\delta}{4}y + \frac{1}{4}\delta\dot{x} + \frac{1}{St}\left(\frac{x}{2} - \dot{y}\right) \mp \frac{1}{St}, \tag{25}$$

$$\delta = \rho_f/\rho_p, \qquad St = \frac{\rho_p \phi^2}{18\mu}\Omega_0, \tag{26}$$

Downloaded¬22¬May¬2004¬to¬128.111.70.70.¬Redistribution¬subject¬to¬AIP¬license¬or¬copyright,¬see¬http://pof.aip.org/pof/copyright.jsp

where the minus/plus sign holds for heavy/light particles. In these scaled coordinates the terminal velocity is $\pm$ 1 depending upon whether the particle is lighter or heavier than the fluid.

The complementary function for this fourth order linear system is the same as for the case without gravity, and its eigenvalues are not modified by the presence of gravity. Consequently, the complete solution now consists of this complementary function and a particular integral, both of which are again easily evaluated in the complex variable z,

$$z = x + iy = c_1 e^{\lambda_1 t} + c_2 e^{\lambda_2 t} \mp i \frac{1}{Stc}, \tag{27}$$

in which $\lambda_{1,2}$ and c, are given by Eqs. (11)–(12). Thus the ejection/entrapment rate is not modified by the presence of gravity. The trends in the particle motion outlined earlier remain the same, except for two differences. First, the accumulation point for the particles is shifted from the vortex center to a new location given by $\mp i\,(1/cSt)$. Light particles follow an inward logarithmic spiral which asymptotically approaches this new location. Heavy particles placed a small distance away from the equilibrium location follow an outward spiral. Second, the presence of gravity modifies the constants c_1 and c_2.

The location of the focus (x_0, y_0) of the logarithmic spiral can be obtained from the particular integral of Eq. (27),

$$x_0 + iy_0 = \mp i \frac{1}{Stc} \tag{28}$$

or

$$x_0 + iy_0 = \mp \left(\frac{-8}{St^2\delta^2 + 4} + i \frac{4St\delta}{St^2\delta^2 + 4} \right), \tag{29}$$

where the minus sign holds for heavy particles and the plus sign for light ones. It is possible to eliminate the factor $St\delta$ from the above equation and represent y_0 as a function of x_0,

$$y_0 = \mp \sqrt{-x_0(\mp 2 + x_0)}, \tag{30}$$

where again the minus sign holds for heavy particles and the plus sign for light ones. The loci of the resulting spiral foci are plotted in Fig. 5.

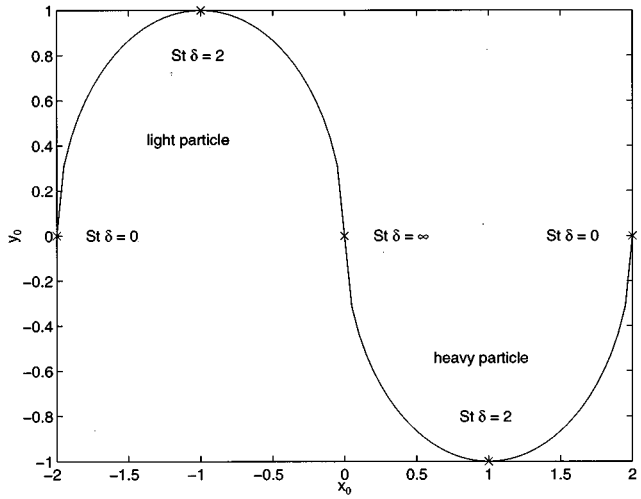

FIG. 5. Focus on the logarithmic spirals plotted as a parametric function for the entire range of the factor $St\delta$. The branch on the right is for heavy particles ($\delta<1$), while that on the left is for light ones ($\delta>1$). Light particles spiral towards the focal point, whereas heavey ones spiral away from it.

IV. POINT VORTEX MODEL

This model is used as a basis for analyzing the transport of particles in the outer regions of a vortex, where the azimuthal velocity of the fluid decreases with increasing distance from the vortex center. The fluid velocity components are

$$u_\theta = \frac{\Gamma_0}{2\pi r}, \qquad u_r = 0, \tag{31}$$

where Γ_0 denotes the circulation of the vortex. There are no characteristic velocity or time scales associated with the fluid motion. The only length scale contained in the problem is the particle's initial distance from the vortex center. However, using this scale in making the equations dimensionless would result in identical particles having different values of St, depending on their initial location. Such a situation should be avoided, so that we use an arbitrary length scale γ instead.

By analyzing the particle dynamics in polar coordinates, some interesting simplifications in the particle equations can be obtained, if we follow Manton[14] and Auton[18] and replace the derivative with respect to the particle $(d\mathbf{u}/dt)$ in the added mass term of Eq. (1) by the total derivative with respect to the fluid $(D\mathbf{u}/Dt)$. The particle motion is then governed by the fourth order system,

$$(1 + \tfrac{1}{2}\delta)\ddot{r} = -\frac{\dot{r}}{St} + (1-\delta) r \dot{\theta}^2, \tag{32}$$

$$\left(1 + \frac{1}{2}\delta\right) \frac{d(r^2\dot{\theta})}{dt} = \frac{1}{St}\left(\frac{1}{2\pi} - r^2\dot{\theta}\right), \tag{33}$$

$$\delta = \rho_f/\rho_p, \qquad St = \frac{\rho_p \phi^2}{18\mu} \frac{\Gamma_0}{\gamma^2}. \tag{34}$$

A preliminary numerical investigation by Lázaro and Lasheras[31] in the heavy particle limit ($\delta \to 0$), for which the pressure gradient and added mass terms drop out, demonstrates that particles of larger size are ejected farther. In the present study we address the entire range between the heavy particle and the bubble limits. Equation (33) can be integrated once to obtain

$$r^2\dot{\theta} = \frac{1}{2\pi} + c\, \exp\left(-\frac{t}{St(1+\delta/2)} \right). \tag{35}$$

The integration constant c is identically equal to zero, provided that the initial azimuthal velocity of the particle is equal to that of the surrounding fluid. This assumption is quite realistic for small values of St, for which the initial velocity difference decays quickly. For larger St values, however, this velocity difference may be felt for longer times. Along the radial direction, the equation describing particle motion can be obtained by substituting Eq. (35) into

Downloaded¬22¬May¬2004¬to¬128.111.70.70.¬Redistribution¬subject¬to¬AIP¬license¬or¬copyright,¬see¬http://pof.aip.org/pof/copyright.jsp

Eq. (32), which results in the decoupling of the equations in the r- and θ-directions. By assuming $c=0$, i.e, by setting the initial azimuthal velocity of the particle equal to that of the surrounding fluid, we get

$$\left(1+\frac{1}{2}\delta\right)\ddot{r}=-\frac{\dot{r}}{St}+(1-\delta)\frac{(1/(2\pi))^2}{r^3}. \tag{36}$$

From left to right, the three terms correspond to one component of the inertial force, drag force, and a combination of centrifugal, pressure gradient, and added mass forces. The above equation can be rescaled with the time and length scales

$$T=St(1+\delta/2), \qquad L=\left(\frac{St}{2\pi}\right)^{1/2}|1-\delta|^{1/4}(1+\delta/2)^{1/4}, \tag{37}$$

to obtain

$$\ddot{r}=\begin{cases}-\dot{r}\pm 1/r^3, & \text{if } \delta\neq 0,\\ -\dot{r}, & \text{if } \delta=0,\end{cases} \tag{38}$$

where the plus sign holds for heavy particles and the minus sign for light ones. From both Eq. (36) and Eq. (38), it is clear that for vanishing initial radial velocity light particles move inward while heavy ones move outward. The advantage of the rescaled Eq. (38) is that it does not have any parameters, i.e., the solution for all values of St and δ can be obtained by merely changing the initial conditions. However, we have been unable to find a closed form solution to Eq. (38). Consequently, one needs to solve it by numerical or approximate methods. Hence, a disadvantage of the rescaled Eq. (38) is that, unlike Eq. (36), it is not conducive to any type of perturbation expansion in terms of St and δ.

Some qualitative scaling arguments based on Eq. (38) are helpful. These scaling arguments can then be used to study Eq. (36) in more detail for small and large values of St. In addition, small deviations from $\delta=1$ can be addressed as well, in order to investigate the effect of slight density variations on the particle's ability to track the fluid motion.

Throughout this section on the point vortex model, we assume that the initial radial velocity of the particle vanishes, i.e., $\dot{r}(t=0)=0$. Therefore, initially the term on the lhs of the equation (called ''inertia term'' for short) has to balance the last term on the rhs (called ''centrifugal term'' for short). This balance, however, may not hold for all times. Equation (38) allows us to find the proper balance as $t\to\infty$. There are three possibilities: Inertia balances drag, inertia balances the centrifugal force, or drag balances the centrifugal force. For a balance between inertia and drag,

$$\ddot{r}=-\dot{r}, \tag{39}$$

so that

$$r=c_1e^{-t}+c_2. \tag{40}$$

For this $r(t)$ relationship, however, the neglected centrifugal term is of the form

$$1/r^3\sim e^{3t}, \tag{41}$$

and would overtake the other two eventually. Consequently, inertia and drag do not provide the proper balance for long times. If instead inertia is balanced by the centrifugal forces, we obtain

$$\ddot{r}=\pm 1/r^3, \tag{42}$$

resulting in

$$r=\sqrt{\pm(2c_1t+c_2)^2+1}. \tag{43}$$

With this solution, however, the neglected term ($\dot{r}$) would again overake the other two terms for long times. Consequently, this balance is invalid as well. That only leaves the balance between drag and centrifugal forces,

$$\dot{r}=\pm 1/r^3, \tag{44}$$

which leads to

$$r=(c\pm t)^{1/4}. \tag{45}$$

In this case, the inertia term given by $\ddot{r}=-3(c\pm t)^{-7/4}/16$ indeed becomes negligible for long times, confirming this balance as the only valid one. The plus sign holds for heavy particles, while the minus sign holds for light ones. It should be noted that for light particles there is a possibility that the balance between drag and centrifugal forces may never be established, if the particle reaches the vortex center in a finite time. This point will be discussed in more detail below. Heavy particles of all St values always attain this final balance.

For small values of St, some interesting asymptotic results can be obtained, as will be discussed in the following.

A. $St\sim\epsilon$

1. Heavy particles

The force balances discussed earlier, i.e., the initial balance between inertia and centrifugal forces and the long time asymptotic balance between drag and centrifugal forces, are reflected in the ''exact'' numerical solutions of Eq. (36). Figure 6 shows the magnitude of these three forces acting on a particle with a density ratio of 0.1 and $St=0.1$. The particle is released at a radius of 0.3 units with the velocity of the surrounding fluid. As discussed above, the centrifugal forces are initially balanced by inertia, whereas for long times they are in balance with the drag. This behavior is qualitatively the same for all density ratios smaller than one.

Hence it is possible to obtain the inner (short time) solution, to first order, by balancing inertia with the centrifugal force. But this balance lasts only up to $t\approx 10^{-2}$. Therefore, neglecting it is not likely to add a significant error to the particle displacement for longer times, so that an approximate solution to Eq. (36), valid for all but very small times, can be obtained by balancing drag with the centrifugal force,

$$r=(r_0^4+4(1-\delta)ktSt)^{1/4}. \tag{46}$$

Here

$$k=\frac{1}{(2\pi)^2}. \tag{47}$$

For small times the radial particle motion is proportional to t, while for later times it is proportional to $t^{1/4}$. Further, if

Downloaded¬22¬May¬2004¬to¬128.111.70.70.¬Redistribution¬subject¬to¬AIP¬license¬or¬copyright,¬see¬http://pof.aip.org/pof/copyright.jsp

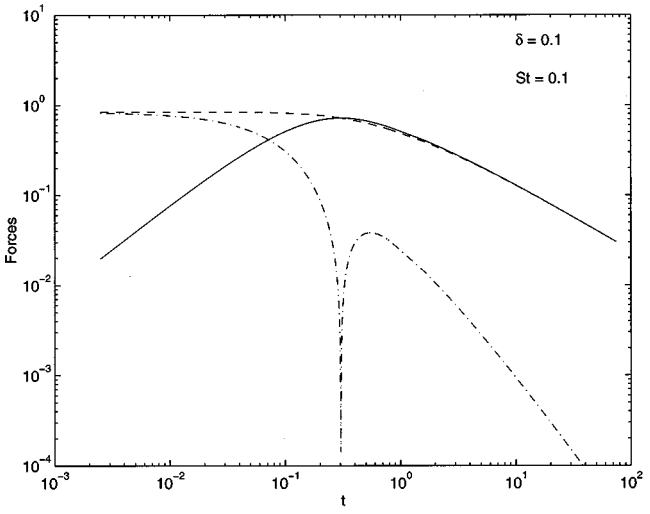

FIG. 6. $St=0.1$, $\delta=0.1$. Absolute values of all three forces as function of time. Dashed lines—centrifugal force; solid line—drag; dash–dot—inertia. The balance is initially between inertia and centrifugal forces, while later it is between drag and centrifugal forces. This behavior remains qualitatively the same for all values of δ below unity.

either the particle density or the Stokes number are increased, the radial particle location grows more rapidly.

By scaling time with $4|1-\delta|kSt$,

$$\tau=4|1-\delta|ktSt, \tag{48}$$

Eq. (46) leads to the scaling law,

$$r=(r_0^4\pm\tau)^{1/4}, \tag{49}$$

where the plus sign holds for heavy particles and the minus sign for light ones. Below, it will become clear that this law is modified for large values of St.

This particle parameter independent scaling law, plotted in Fig. 7 for two initial conditions $r_0=0.3$ and $r_0=0.6$, is in excellent agreement with the ''exact'' numerical solutions. These were obtained by integrating the governing equations

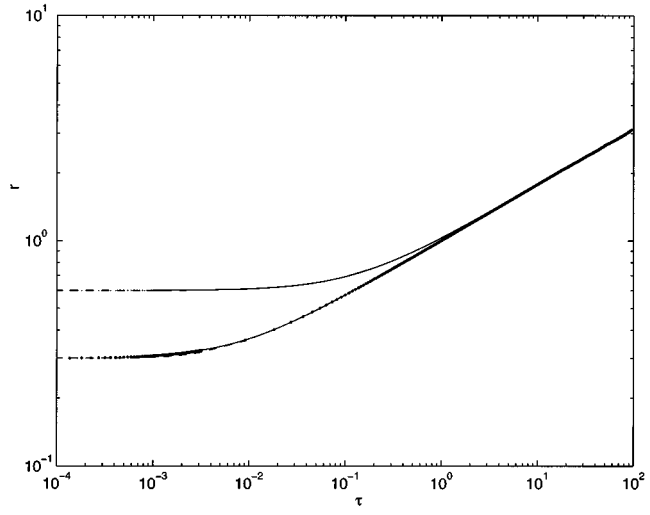

FIG. 7. $St=0.1$. Radial displacement of heavy particles. The scaling law of Eq. (50) is plotted as solid lines for two initial conditions: $r_0=0.3$ and $r_0=0.6$. ''Exact'' numerical solutions represented by (i) dashed lines for $\delta=0.1$ and (ii) dotted lines for $\delta=0.9$ are almost identical to the scaling law.

using a fourth order Runge–Kutta scheme. In obtaining the numerical solutions, for each initial condition, two values of δ $(=0.1,0.9)$ were chosen while the Stokes number was maintained at $St=0.1$.

Whether or not particles accumulate in the point vortex depends on the divergence of the particle velocity field: Particles accumulate only in regions where this divergence is negative. The Eulerian description of the particle motion can be obtained on the basis of the above Lagrangian information. Equation (46) yields the particle velocity as

$$\dot{r}=\frac{(1-\delta)kSt}{(r_0^4+4(1-\delta)ktSt)^{3/4}}, \tag{50}$$

where the denominator in the above equation is identical to r^3. Therefore

$$\dot{r}=v_r=\frac{(1-\delta)kSt}{r^3}, \tag{51}$$

This relationship can be interpreted in a Lagrangian way, i.e., as the velocity of an individual particle as a function of its radial location r, or in a Eulerian way, for example as the local convection velocity of a particle concentration field. With our earlier observation that the azimuthal particle velocity is identical to the fluid velocity, we obtain

$$v_\theta=\frac{1}{2\pi r}, \tag{52}$$

which completes the Eulerian description of the particle velocity field. It indicates that the particle velocity field is uniquely determined by the particle location (r,θ). For the divergence of the particle velocity field we obtain

$$\boldsymbol{\nabla}\cdot\mathbf{v}_p=-\frac{2(1-\delta)St}{r^4}. \tag{53}$$

From the governing equation for the particle concentration field,

$$\frac{\partial c}{\partial t}+\boldsymbol{\nabla}\cdot(\mathbf{v}_p c)=0, \tag{54}$$

we thus obtain

$$\frac{1}{c}\frac{dc}{dt}=-\boldsymbol{\nabla}\cdot\mathbf{v}_p, \tag{55}$$

where d/dt is the total derivative with respect to the particle. This equation states that the relative rate of change of the particle concentration is given by the negative divergence of the particle velocity field. We can hence define an instantaneous accumulation rate, α_r,

$$\alpha_r=\frac{1}{c}\frac{dc}{dt}=-\boldsymbol{\nabla}\cdot\mathbf{v}_p, \tag{56}$$

which for the present case results in

$$\alpha_r=\frac{2(1-\delta)St}{r^4}. \tag{57}$$

The accumulation rate is positive for heavy particles, and it increases with the particle density and St. In the simplified limit of $(\delta\to 0)$, our equations for the point vortex flow cor-

Downloaded¬22¬May¬2004¬to¬128.111.70.70.¬Redistribution¬subject¬to¬AIP¬license¬or¬copyright,¬see¬http://pof.aip.org/pof/copyright.jsp

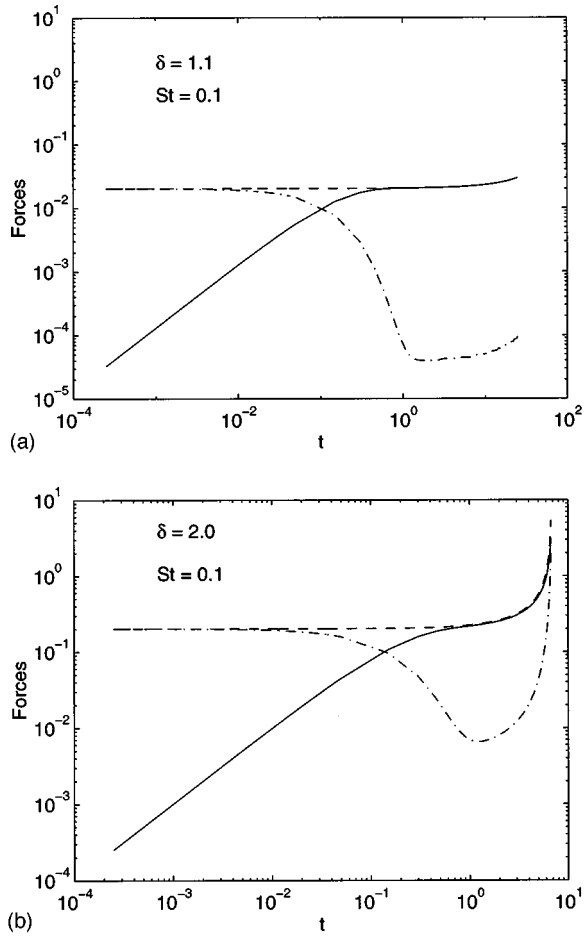

FIG. 8. $St=0.1$, light particle regime. Absolute values of all three forces plotted as a function of time for (a) $\delta=1.1$, and (b) $\delta=2$. Dashed lines—centrifugal force; solid line—drag; dash–dot—inertia. The balance is initially between inertia and centrifugal forces while later it is between drag and centrifugal forces. For larger values of δ, the particle approaches the vortex center faster. As a result, the particle inertia may gain importance at later times, as seen in (b).

respond to those derived by Druzhinin[32] for the Rankine vortex. This author furthermore outlines an equation for the radial particle velocity in an arbitrary axisymmetric vortex. His equation agrees with our Eq. (51) for the case of a point vortex in the heavy particle limit.

2. Light particles

Computational solutions of the full equations for light particles of mass ratios 1.1 and 2.0 display the same qualitative force balances as for heavy particles; cf. Figs. 8(a,b). Figure 8(b) indicates that with increasing δ, the inertia term gains importance for these inward moving particles. Again, the long time solution Eq. (48) approximates the particle motion fairly well; cf. Fig. 9. The scaling law is plotted for two initial conditions of $r_0=0.5$ and $r_0=0.7$. For both initial conditions, in obtaining the numerical solutions, two values of δ ($=1.1,2.0$) were chosen, while the Stokes number was maintained at $St=0.1$. As can be seen from Eq. (46), the radial motion of these light particles becomes stronger if either their density decreases or their Stokes number increases. Accumulation in the regions away from the vortex center

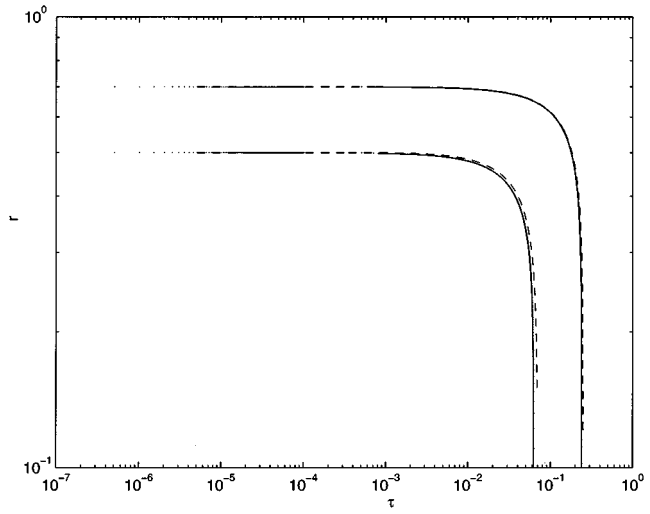

FIG. 9. $St=0.1$. Radial displacement of light particles. The scaling law of Eq. (50) is plotted as solid lines for two initial conditions: $r_0=0.5$ and $r_0=0.7$. ''Exact'' numerical solutions plotted as (i) dotted lines for $\delta=1.1$ and (ii) dashed lines for $\delta=2.0$ are in reasonable agreement with the scaling law.

does not take place, as reflected by the negative accumulation rate. In summary, the transport trends for light particles are again opposite to those for heavy particles.

B. $St\sim 1/\epsilon$

1. Heavy particles

If the initial velocity of the particle is identical to that of the surrounding fluid, the centrifugal force initially again has to balance inertia. In addition, for large times drag again has to balance the centrifugal forces, as discussed earlier. However, it now takes much longer to achieve this final balance, and an intermediate regime in which inertia is balanced by drag can arise, as shown by numerical results for $St=10.0$ and $\delta=0.1$; cf. Fig. 10. Here, the initial particle location is again $r_0=0.3$. This intermediate balance has its origin in the larger radial momentum imparted initially on large St particles by the centrifugal forces. For intermediate times, some of this momentum is dissipated by the drag force. Only after a significant slowing of the particle is the final regime attained, in which drag is balanced by centrifugal forces. Qualitatively similar behavior is observed for all density ratios less than unity.

It is straightforward to obtain a first order approximate solution for short and intermediate times. With $St\sim 1/\epsilon$, Eq. (36) becomes

$$(1+\delta/2)\ddot{r}=-\epsilon\dot{r}+(1-\delta)k/r^3. \tag{58}$$

The inner, short time solution in our expansion expresses the balance between inertia and centrifugal forces, while the intermediate time solution balances inertia and drag. These two solutions can then be matched to arrive at the composite solution.

The initial balance between inertia and centrifugal forces leads to the following inner solution:

Downloaded¬22¬May¬2004¬to¬128.111.70.70.¬Redistribution¬subject¬to¬AIP¬license¬or¬copyright,¬see¬http://pof.aip.org/pof/copyright.jsp

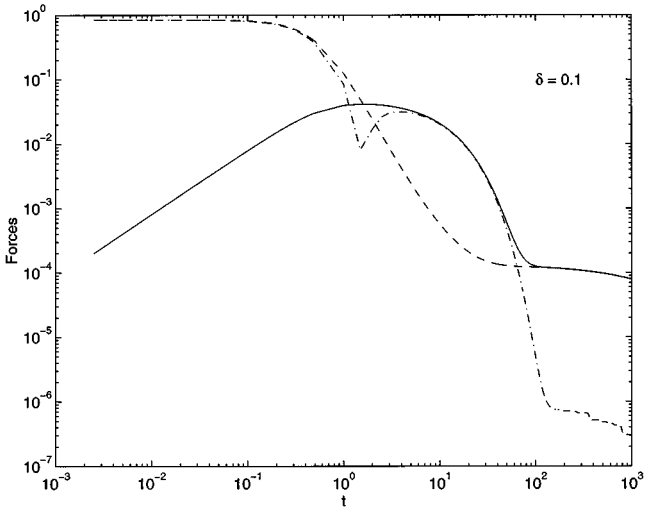

FIG. 10. $St=10.0$, $\delta=0.1$. Absolute values of all three forces plotted against time. Dashed lines—centrifugal force; solid line—drag: dash–dot—inertia. The initial and final balances are the same as those for the small Stokes number case plotted in Fig. 6: Initially, the balance is between inertia and centrifugal forces, while the final balance is between drag and centrifugal forces. There now is a new intermediate regime in which drag and inertia match each other.

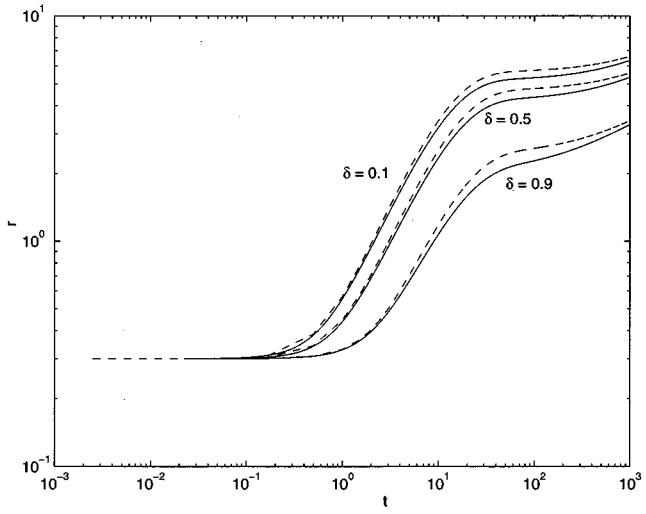

FIG. 11. $St=10$. Radial displacement of heavy particles: ''Exact'' numerical solution (dahsed lines) and asymptotic expansion (solid lines). The expansion is in reasonable agreement with the numerical solution.

$$r_{inner}=\sqrt{r_0^2+\frac{(1-\delta)kt^2}{(1+\delta/2)r_0^2}}. \tag{59}$$

The balance between inertia and drag results in the governing equation for the intermediate regime,

$$(1+\delta/2)\ddot{r}+\dot{r}/St=0,$$

which has the solution

$$r_{inter}=a+b\ \exp\left(\frac{-t}{St(1+\delta/2)}\right).$$

The constants a and b can be evaluated by matching the intermediate and inner solutions, r_{inter} and r_{inner}. Upon matching, the composite solution takes the form

$$r_{c1}=\sqrt{r_0^2+\frac{(1-\delta)kt^2}{(1+\delta/2)r_0^2}}+\frac{(1-\delta)^{1/2}k^{1/2}(1+\delta/2)^{1/2}}{r_0}St(1-e^{-t/(1+\delta/2)St})-t\sqrt{(1-\delta)k/r_0^2(1+\delta/2).} \tag{60}$$

We can proceed to obtain the solution for the outer regime in which drag is balanced by inertia. Similar to the solution for the small St case we obtain

$$r_{outer}=(c+4(1-\delta)ktSt)^{1/4}, \tag{61}$$

where c is a constant to be obtained by matching. The composite expansion valid for all three regimes can now be obtained by matching the above solution with r_{c1} to obtain

$$r_c=\sqrt{r_0^2+\frac{(1-\delta)kt^2}{(1+\delta/2)r_0^2}}-\frac{(1-\delta)^{1/2}k^{1/2}(1+\delta/2)^{1/2}}{r_0}St(e^{-t/(1+\delta/2)St})-t\sqrt{\frac{(1-\delta)k}{r_0^2(1+\delta/2)}}+(c+4(1-\delta)ktSt)^{1/4}, \tag{62}$$

$$c=\frac{(1-\delta)^{1/2}k^{1/2}(1+\delta/2)^{1/2}}{r_0}St. \tag{63}$$

Figure 11 shows that this first order solution agrees reasonably well with the ''exact'' numerical solution. The radial velocity of a particle increases with St, similarly to our earlier findings for the small St regime. This trend agrees with the experimental observations by Laźaro and Lasheras,[7] who find that particles of larger diameter accumulate farther away from the vortex centers.

Within the intermediate range, the two terms with the radical signs in Eq. (60) cancel out for large times. Hence

$$r_{c1}\big|_{t\gg 1}=\frac{(1-\delta)^{1/2}k^{1/2}(1+\delta/2)^{1/2}}{r_0}\times St\left(1-\exp\left(\frac{-t}{(1+\delta/2)St}\right)\right). \tag{64}$$

All particle characteristics can be eliminated from this relationship by rescaling the radial displacement as well as time. Let

$$R=\frac{r}{(1-\delta/2-\delta^2/4)^{1/2}Stk^{1/2}} \tag{65}$$

and

$$T=\frac{t}{(1+\delta/2)St}. \tag{66}$$

We then obtain for the radial displacement,

$$R=\frac{1}{r_0}(1-e^{-T}). \tag{67}$$

Downloaded¬22¬May¬2004¬to¬128.111.70.70.¬Redistribution¬subject¬to¬AIP¬license¬or¬copyright,¬see¬http://pof.aip.org/pof/copyright.jsp

Notice the difference between this scaling law and the one for small Stokes numbers in Eq. (46).

In the limit as $\delta \to 0$, the above arguments further simplify. With

$$R_1 = \frac{r}{Stk^{1/2}} \tag{68}$$

and

$$T_1 = \frac{t}{St}, \tag{69}$$

we obtain

$$R_1 = \frac{1}{r_0}(1 - e^{-T_1}). \tag{70}$$

The scaling relationships of Eqs. (68)–(69) are related to the ones proposed by Laźaro and Lasheras[6] for obtaining a scaling law for heavy particles in unforced mixing layers that does not depend on the particle parameters. These authors scale their particle dispersion measure (0.1–0.9 level thickness) and the downstream distance x_d by $\rho_p \phi^2/(18\mu)$. This factor, when nondimensionalized, becomes our St. Keeping in mind that their dispersion measure and x_d directly correspond to our radial displacement and time, the relationship with the above scaling becomes obvious.

Let us compare the radial displacement expressed by Eq. (64) for two particles with identical parameters but starting at different locations r_{01} and r_{02} with $r_{01} < r_{02}$. The particle at the smaller initial radius r_{01} eventually moves to a larger radial location. This leads to the formation of concentration waves with propagating crests. This behavior results from the fact that the particle starting at a smaller radius obtains a higher angular momentum from the surrounding fluid, which eventually drives it to larger radii. It leads to a situation where two particles at the same radial location can have different velocities, so that the particle velocity field cannot be described as a single-valued function of the radius.

Computations shown in Fig. 12 demonstrate that particles of intermediate St accumulate optimally in the point vortex flow field. The figure shows particle concentrations for $\delta = 0$ and $St = 0.1$, 1, and 10. To obtain these figures, 90 000 particles were seeded uniformly in the annular region bounded by $r_1 = 0.3$ and $r_2 = 4$, with a velocity equal to the local fluid velocity. Subsequently, these particles were tracked until $t = 10$ by numerically integrating Eqs. (32) and (33) with a fourth order Runge–Kutta scheme.

We next address the question of why particles of intermediate values of St are optimally accumulated. For accumulation to occur in a region, more particles should be driven into that region than that driven out. Let us consider an annular region bounded by the two radii, r_1 and r_2 $(= r_1 + \Delta r)$. Heavy particles enter this region through the surface $r = r_1$ and exit it through the surface $r = r_2$. Let us first treat the small-St regime. Recall that for small values of St, the drag force is balanced by the centrifugal force, which decreases rapidly with increasing r, thereby causing accumulation in an initially constant concentration field: because the centrifugal force is higher at $r = r_1$ than that at $r = r_2$, it forces more particles to enter the given region through the surface r_1 than that it forces to exit through the surface $r = r_2$. Further, the velocity of the particles entering at $r = r_1$ is by Eq. (51), more than that of those exiting at $r = r_2$. Stokes drag tends to oppose this accumulation because it, being proportional to the velocity, is higher for the particles that are entering the given region, i.e., it hinders the entering particles more than it hinders the exiting particles. As St is increased, the drag decreases and as a result the centrifugal force can accumulate the particles more effectively. Nevertheless, the accumulation remains somewhat limited in this small St regime, due to the relatively large drag force.

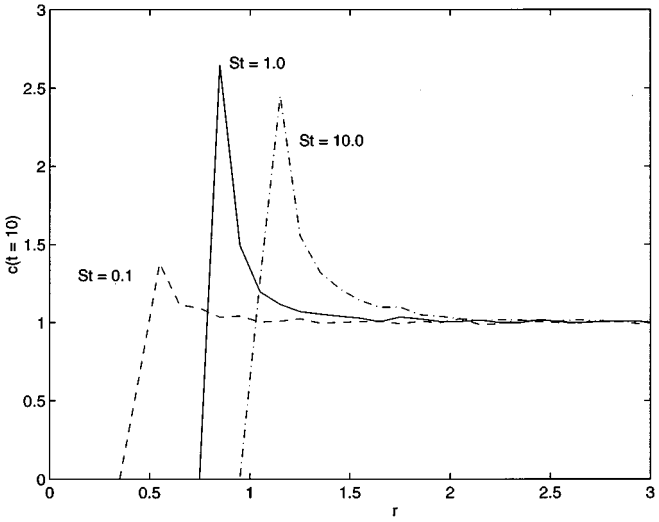

FIG. 12. Ratio of the particle concentration to the initial concentration in a point-vortex flow, plotted for $\delta = 0.0$ and three values of St: Dashed line—$St = 0.1$; solid line—$St = 1.0$; dash–dot—$St = 10.0$. Particles with intermediate values of St experience optimal accumulation.

In the large St regime, initially the centrifugal force balances inertia. The centrifugal force again causes accumulation. However, this balance between inertia and centrifugal force holds for only short durations. In the intermediate regime, the centrifugal force is small, and the balance is between inertia and drag. Consequently, the significance of the centrifugal force decreases as we increase St from small to large values. The drag force, which opposes the accumulation, also decreases, since it is inversely proportional to St. In other words, the forces causing accumulation and the force opposing accumulation both become smaller as St is increased. We can therefore conclude that the difference between these two opposing forces is maximized for intermediate values of St, thereby leading to the observed optimal accumulation for particles with intermediate St.

2. Light particles

Again we start with numerical simulations to obtain the force balances (see Fig. 13). Light particles approach the center of the point vortex rapidly and reach the origin in a finite time because of the unphysical singularity at the origin. As a result, there is not enough time for the particle to display the second and third balances observed in the previous section on heavy particles. The balance is between inertia

Downloaded¬22¬May¬2004¬to¬128.111.70.70.¬Redistribution¬subject¬to¬AIP¬license¬or¬copyright,¬see¬http://pof.aip.org/pof/copyright.jsp

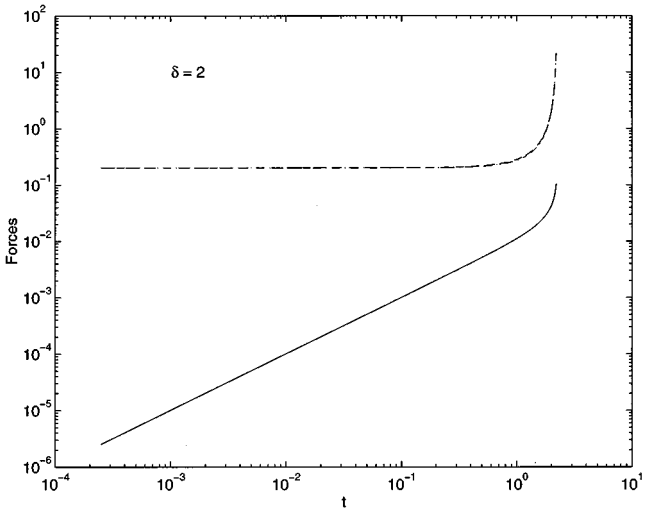

FIG. 13. $St=10$, $\delta=2$: The absolute values of all three forces plotted againts time. Dashed line—centrifugal force; solid line—drag; dash–dot—inertia. The balance is always between inertia and centrifugal forces. These light particles approach the vortex center in a finite time and therefore do not remain in the flow field long enough to attain the final balance observed in Figs. 6, 8, and 10.

and centrifugal forces for all times. The first order solution is the same as the inner solution from the previous section expressed by Eq. (59). These solutions, plotted for three different density ratios, are in good agreement with the numerical solutions; Fig. 14. In this case, particles are rapidly forced towards the origin and hence no accumulation is possible.

C. $\delta=1+\epsilon$

This expansion is performed to analyze if the particles used in DPIV are robust with respect to density variations. On substituting $\delta=1+\epsilon$ in Eq. (36),

$$\left(\frac{3+\epsilon}{2}\right)\ddot{r}=-\frac{\dot{r}}{St}-\frac{\epsilon k}{r^3}, \tag{71}$$

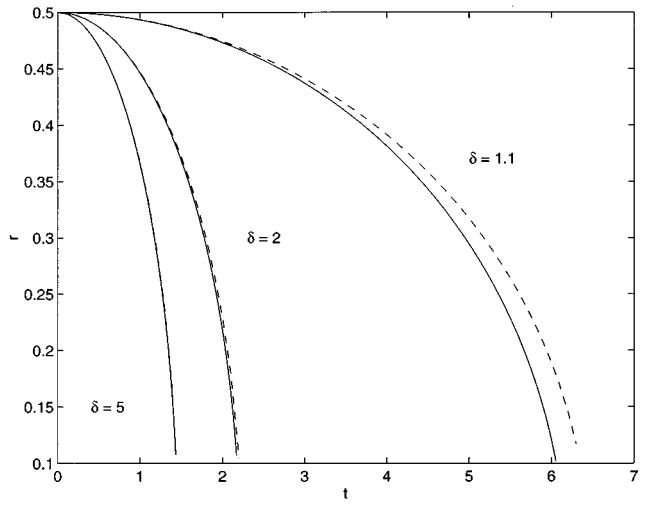

FIG. 14. $St=10$. Radial displacement of light particles. ''Exact'' numerical solution (dashed lines) and asymptotic expansion (solid lines). The expansion is in reasonable agreement with the numerical solution. Particles approach the vortex center faster if their mass is decreased (or $\delta\uparrow$).

where $k=1/(2\pi)^2$. We can expand the solution as a power series in (ϵ),

$$r=R_0+\epsilon R_1+\epsilon^2 R_2+\ldots\ . \tag{72}$$

To first order,

$$3\ddot{R}_0/2=-\dot{R}_0/St, \qquad R_0(0)=r_0, \qquad \dot{R}_0(0)=0. \tag{73}$$

Therefore, to first order the drag balances inertia. The $O(\epsilon)$ equation is

$$3\ddot{R}_1/2=-\dot{R}_1/St-k/R_0^3, \qquad R_1(0)=0, \quad \dot{R}_1(0)=0. \tag{74}$$

The solution to $O(\epsilon)$ is

$$r=r_0+\epsilon\frac{3kSt^2}{2r_0^3}(1-e^{-2t/3St})-\epsilon\frac{kSt}{r_0^3}t. \tag{75}$$

The second term on the rhs of the above solution is negligible for small values of St. Therefore the error in tracking the fluid is

$$e=|r-r_0|=|\epsilon|\frac{kSt}{r_0^3}t+O(\epsilon^2). \tag{76}$$

The same error can be obtained from the small St expansion performed earlier by letting $\delta=1+\epsilon$ in Eq. (46). Thus the error increases if the particle Stokes number is increased.

We next analyze the effect of small deviations in the initial velocity on the tracking capability of the particle. With $\delta=1$, Eq. (36) becomes

$$3\ddot{r}/2=\dot{r}/St, \tag{77}$$

$$r(0)=r_0, \qquad \dot{r}(0)=\epsilon.$$

The resulting error is

$$e=|r-r_0|=3|\epsilon|St(1-e^{-2t/3St})/2.$$

Hence, the particle deviates by a distance approximately proportional to St, again provided that history effects are negligible.

V. STAGNATION POINT ZONE

The flow in this zone is represented by a linear strain field,

$$u_x=\alpha_0 y, \qquad u_y=\alpha_0 x, \tag{78}$$

where α_0 is the strain rate. In the absence of gravity, the characteristic time scale of this flow field is the inverse of the strain rate $(1/\alpha_0)$, whereas a characteristic length scale does not exist. In order to nondimensionalize the governing equations, we hence choose an arbitrary length scale γ. The particle motion is then governed by the equations

$$\left(1+\frac{1}{2}\delta\right)\ddot{x}=\delta x+\frac{1}{2}\delta\dot{y}+\frac{1}{St}(y-\dot{x}), \tag{79}$$

$$\left(1+\frac{1}{2}\delta\right)\ddot{y}=\delta y+\frac{1}{2}\delta\dot{x}+\frac{1}{St}(x-\dot{y})-\frac{1-\delta}{Fr^2}, \tag{80}$$

Downloaded¬22¬May¬2004¬to¬128.111.70.70.¬Redistribution¬subject¬to¬AIP¬license¬or¬copyright,¬see¬http://pof.aip.org/pof/copyright.jsp

$$\delta=\rho_f/\rho_p, \qquad St=\frac{\rho_p\phi^2}{18\mu}\alpha_0, \qquad Fr^2=\frac{\gamma{\alpha_0}^2}{g}. \tag{81}$$

Both Ramarao and Tien[16,17] and Morrison[15] studied this problem in detail. By employing Laplace transforms, the latter author was able to derive a closed form solution that accounts for the old form of the Basset history term. In light of the recent findings discussed above regarding the decreased importance of the Basset history term, however, a fresh look at the the dynamics of particles across the entire density spectrum in stagnation point flows is needed.

Equations (79) and (80) can be decoupled along the strain axes ξ $[=(x+y)/\sqrt{2}]$ and η $[=(y-x)/\sqrt{2}]$

$$\left(1+\frac{1}{2}\delta\right)\ddot{\xi}=\delta\xi+\frac{1}{2}\delta\dot{\xi}+\frac{1}{St}(\xi-\dot{\xi})-\frac{1-\delta}{Fr^2\sqrt{2}}, \tag{82}$$

$$\left(1+\frac{1}{2}\delta\right)\ddot{\eta}=\delta\eta-\frac{1}{2}\delta\dot{\eta}-\frac{\eta}{St}-\frac{\dot{\eta}}{St}-\frac{1-\delta}{Fr^2\sqrt{2}}. \tag{83}$$

These equations represent a set of two decoupled linear dynamical systems. We first study the solution along the compressional strain axis η,

$$\eta=c_1e^{\lambda_1 t}+c_2e^{\lambda_2 t}+l_0, \tag{84}$$

$$l_0=\frac{1-\delta}{(\delta^2-1/St)\sqrt{2}Fr^2}, \tag{85}$$

$$\lambda_{1,2}=\frac{-(1/St+\delta/2)\pm\sqrt{(1/St+\delta/2)^2-4(1+\delta/2)(1/St-\delta)}}{2(1+\delta/2)}. \tag{86}$$

While λ_2 always has a negative real part, λ_1 has a positive real part if $St\delta>1$, which indicates that the particle moves against the flow towards infinity. This behavior, already observed by Morrison, is caused by the pressure gradient force, which overcomes the opposing influence of the drag. Under such circumstances, the third condition in Eq. (2) may not hold and as a result, the solution expressed by (84) may be incorrect.[30]

If, on the other hand, $Re(\lambda_1)<0$, the particles converge to a line parallel to $\eta=0$, where they accumulate. The distance of this line from $\eta=0$, which increases with gravity, is determined by the last term in Eq. (84). The rate of approach is determined by the largest real part λ_r of the eigenvalues, which is plotted in Fig. 15(a). For a given density ratio (δ), the rate of approach for heavy particles is maximized for intermediate St values. Light particles, on the other hand, do not display any optimal trend in the rate of approach: Their rate of approach continues to decrease as St is increased.

Figure 15(b) shows the imaginary part of the largest eigenvalues. A nonzero value for a given δ and St indicates oscillatory particle motion. Heavy particles exhibit this behavior for a range of Stokes numbers, with maximum frequencies for intermediate St values.

The behavior of the present second order linear system can be interpreted as a damped harmonic oscillator. By rewriting Eq. (83), we obtain

$$m\ddot{\eta}+c\dot{\eta}+k\eta=-\frac{1-\delta}{\sqrt{2}Fr^2},$$
$$m=1+\frac{\delta}{2}, \qquad c=\frac{1}{St}+\frac{\delta}{2}, \qquad k=\frac{1}{St}-\delta. \tag{87}$$

The ''damping'' c is provided by both the Stokes drag and the added mass term. The Stokes drag also contributes to the ''spring-constant'' k in a positive fashion, as it tends to move the particle towards the stagnation point. The pressure gradient, on the other hand, lowers the spring constant by driving the particle away from the stagnation point. The added mass increases the ''mass'' m of the oscillator. The constant forcing provided by gravity does not alter the particle damping characteristics.

Critical damping occurs when the imaginary part of the eigenvalue vanishes. By setting the discriminant in Eq. (86) equal to zero

$$\left(\frac{1}{St}\right)^2+\left(\frac{3\delta}{2}\right)^2-\frac{\delta}{St}-\frac{4}{St}+4\delta=0,$$

we can solve for St,

$$St_{1,2}=\frac{\delta+4\mp\sqrt{8(2-\delta^2-\delta)}}{8\delta+9\delta^2/2}. \tag{88}$$

Between these two values of St, the particle exhibits oscillatory motion. If $\delta>1$, there is no physically meaningful solution for St, indicating that light particles never undergo critical damping. Light particles are overdamped if $St\delta<1$. For $St\delta>1$, on the other hand, they give rise to a negative spring constant. Consequently, light particles never undergo an oscillatory motion.

It is interesting to study the dynamics of heavy particles as St varies and δ is held constant. In the limit as $St\to 0$, heavy particles behave like fluid particles. As St is increased, they approach the accumulation line more and more rapidly unitl St_1 is reached [see Fig. 15(a)]. At St_1, they are critically damped and their rate of approach is maximized. For $St_1<St<St_2$, the particles are underdamped and exhibit oscillatory motion, so that they can cross $\eta=0$ in finite time.

Downloaded¬22¬May¬2004¬to¬128.111.70.70.¬Redistribution¬subject¬to¬AIP¬license¬or¬copyright,¬see¬http://pof.aip.org/pof/copyright.jsp

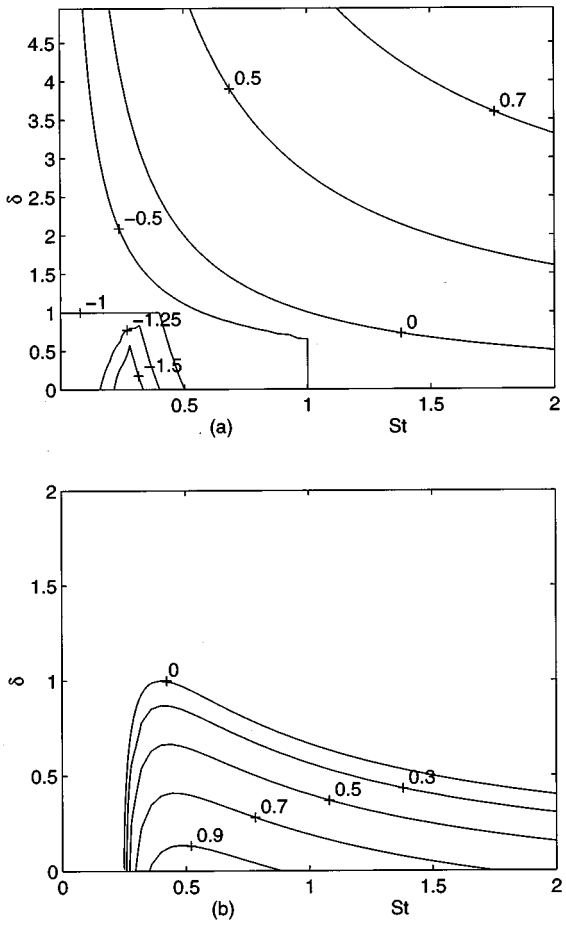

FIG. 15. Stagnation point flow: Contour plots of (a) real and (b) imaginary parts of the eigenvalue with the largest real component. Particles with a negative real part accumulate along the extensional strain axis. For a range $St_1 < St < St_2$, heavy particles oscillate, as can be seen from the nontrivial values for the imaginary part. A neutrally buoyant particle ($\delta=1$) can track the fluid motion accurately only if $St<2/5$. Notice that if this condition holds, $\lambda_r=-1$, so that the particle approaches the stagnation point at the same rate as the fluid. If this condition is not satisfied, the particle approaches the stagnation point more slowly than the field.

At St_2, they are again critically damped. Subsequently, for $St_2<St<1/\delta$ the particles are overdamped again, and for $St>1/\delta$ they diverge to infinity.

While previous studies by Morrison,[15] Ramarao and Tien[17] and Matsufuji and Hasegawa[33] (for $\delta\rightarrow 0$) observed oscillatory behavior beyond a critical value of St, the present results indicate an upper limit to this oscillatory regime, beyond which the pressure gradient force is strong enough to suppress any oscillations. For $\delta=0$, the value of St_1 is in agreement with the analyses by Matsufuji and Hasegawa[33] and Martin and Meiburg.[3] As δ is increased from zero to unity, the St value for optimal rate of approach (St_1) increases. For the case of $\delta=1$, which is of interest in DPIV studies, the eigenvalues are real,

$$\lambda_1=-\frac{2}{3St}+\frac{2}{3}, \qquad \lambda_2=-1,$$

so that we obtain for the trajectory of a neutrally buoyant particle starting at η_0,

$$\eta=c_1e^{\lambda_1 t}+c_2e^{-t}.$$

Here c_1 and c_2 are constants that depend on the initial velocity of the particle. The trajectory of a fluid particle starting at the same location is

$$\eta_{fluid}=\eta_0e^{-t}.$$

Comparing η_{fluid} with η provides as a necessary condition for the particle's ability to track the fluid motion accurately,

$$\lambda_1<-1. \tag{89}$$

This condition translates to

$$St<2/5. \tag{90}$$

Under this condition, the maximum eigenvalue of the neutrally buoyant particle is always the same as that of the fluid.

VI. DISCUSSION AND SUMMARY

In order to gain an improved understanding of the different mechanisms responsible for the dispersion trends observed in vortical flows, we have investigated three simple flow fields: solid body vortex, point vortex, and stagnation point flow. These situations model the cores of concentrated vortices, their outer regions, and irrotational regions in between vortices.

For all three model flows, we were able to reduce the governing fourth order system to two second order equations. In particular, for the vortex core region we obtain a second order linear system for a complex variable. The point vortex situation translates into a nonlinear system for the radial motion of the particles, while for the linear strain field, two linear decoupled second order equations are derived for the motion along each strain axis. These simplifications allow us to identify several new dispersion trends, and to obtain an improved understanding of others observed before. Most importantly, in the present investigation we address the entire range of density ratios, in contrast to most earlier studies.

For heavy particles in a solid body vortex, the centrifugal force is the only force pointing away from the vortex center, with pressure gradient, added mass, and Stokes drag force all pointing inward. As St is increased, both the inward and the outward forces decrease. However, the difference between them reaches a maximum for intermediate St values, resulting in optimal ejection at these values of St. The rotation rate of heavy particles is shown to be less than that of the surrounding fluid. Analytical expressions for both the ejection rate and the rotational frequency demonstrate the above behavior.

In many ways, light particles show the exact opposite behavior to heavy ones. They are entrapped into the vortex, at a rate that reaches a maximum for intermediate values of St. Here both the inward and the outward forces increase with increasing St, while their difference is maximized at these intermediate values.

The point vortex flow can be analyzed by perturbation expansions for both small and large values of the St. In agreement with previous experimental and numerical studies on various kinds of free shear flows, heavy particles are shown to accumulate in the outer vortical regions. For a fixed density ratio, the rate of accumulation is optimal for interme-

Downloaded¬22¬May¬2004¬to¬128.111.70.70.¬Redistribution¬subject¬to¬AIP¬license¬or¬copyright,¬see¬http://pof.aip.org/pof/copyright.jsp

diate St values. While the centrifugal force is shown to cause this accumulation, the drag force tends to oppose it. Their net balance at intermediate St values results in the above optimal accumulation.

For large St values, a scaling law for the radial displacement is derived, which in the heavy particle limit corresponds to the scaling argument derived by Lazaro and Lasheras[6] from their experiments on the dispersion of heavy particles in unforced mixing layers.

For stagnation point flows, the well-known result of optimum accumulation for heavy particles of intermediate size is extended by deriving an analytical expression for the optimal St value as a function of the density ratio. In the heavy particle limit, this expression is consistent with previous results. In addition, we identify an upper St limit to the underdamped range, beyond which the motion ceases to be oscillatory. These trends are analyzed in terms of damped harmonic oscillators.

Interesting dynamical behavior can furthermore be observed for nearly neutrally buoyant particles, and for their tracking errors due to density mismatches. For stagnation point flows in particular, a restriction on St exists, beyond which the tracking error increases exponentially.

While the above results add to our general understanding of the dynamics of particle laden flows, we have to keep in mind that they were based on a series of simplifying assumptions, such as two-dimensional flow, dilute particle concentration fields, negligible history effects, and one-way coupling. Full Navier-Stokes simulations that account for the effect of the particles on the flow field will certainly lead to observations of additional important phenomena.

ACKNOWLEDGMENTS

The authors gratefully acknowledge support by the National Science Foundation under Grant No. CTS-9196004 and in the form of an equipment grant, and by the Electric Power Research Institute. Computing resources were provided by the San Diego Supercomputer Center.

APPENDIX: ROTATION RATE IN A SOLID BODY VORTEX

Here we prove that, if St is increased from zero to infinity, the long term rotation rate of particles present in a solid body vortex, increases iff the particles are light and it decreases iff the particles are heavy.

The function $\dot{\theta}$ continues to increase as St is increased iff $d\dot{\theta}/d(St)$ remains positive and it continues to decrease iff $d\dot{\theta}/d(St)$ remains negative. Thus $d\dot{\theta}/d(St)$ should not change sign when St is varied from zero to infinity. The rotation rate may be expressed as

$$\dot{\theta}=\frac{\delta/4+\sqrt{(-d+\sqrt{d^2+f^2})/2}}{2(1+\delta/2)}, \tag{A1}$$

$$d=\frac{1}{St^2}-\frac{9\delta^2}{16}-\delta, \tag{A2}$$

$$f=\frac{\delta}{2St}+\frac{2}{St}. \tag{A3}$$

We require that the derivative $d\dot{\theta}/d(St)$ does not change sign for both light ($\delta>1$) and heavy ($\delta<1$) particles. We prove this by showing that the sign changes iff $\delta=1$ and that this sign change does not depend on St. If primes denote differentiation with respect to St, then

$$\dot{\theta}'=0, \tag{A4}$$

$$\Rightarrow -d'\sqrt{d^2+f^2}+dd'+ff'=0, \tag{A5}$$

$$\Rightarrow f^2(d'^2-f'^2)-add'ff'=0, \tag{A6}$$

$$\Rightarrow \frac{(\delta/2+2)^2}{St^4}[(\delta-1)(\delta+2)]=0, \tag{A7}$$

$$\Rightarrow \delta=1, \qquad \text{the other root } \delta=-2 \text{ is meaningless.} \tag{A8}$$

Since $d\dot{\theta}/d(St)$ can be zero only for $\delta=1$, it cannot change its sign for either heavy or light particles. As a result, after showing computationally for at least one data point that the derivative is negative for heavy particles and positive for light particles, one can conclude that $\dot{\theta}$ continues to decrease if the particle is heavy, and to increase if the particle is light.

[1] C. T. Crowe, R. A. Gore, and T. R. Troutt, Particle dispersion by coherent structures in free shear flows,'' Part. Sci. Technol. **3**, 149 (1985).
[2] R. Chein and J. N. Chung, ''Effects of vortex pairing on particle dispersion in turbulent shear flows,'' Int. J. Multiphase Flow **13**, 785 (1987).
[3] J. Martin and E. Meiburg, ''The accumulation and dispersion of heavy particles in forced two-dimensional mixing layers. Part 1: The fundamental and subharmonic cases,'' Phys. Fluids **6**, 1116 (1994).
[4] N. Raju and E. Meiburg, ''The accumulation and dispersion of heavy particles in forced two-dimensional mixing layers. Part 2: The effect of gravity,'' Phys. Fluids **7**, 1241 (1995).
[5] S. Aggarwal and Y. Xiao, ''Effect of external forcing on droplet dispersion in a developing shear layer,'' J. Prop. Power **10**, 395 (1994).
[6] B. J. Lázaro and J. C. Lasheras, ''Particle dispersion in the developing free shear layer. Part 1, unforced flow, J. Fluid Mech. **235**, 143 (1992).
[7] B. J. Lázaro and J. C. Lasheras, ''Particle dispersion in the developing free shear layer. Part 2, forced flow,'' J. Fluid Mech. **235**, 179 (1992).
[8] E. K. Longmire and J. K. Eaton, ''Structure and control of particle-laden jet,'' J. Fluid Mech. **236**, 217 (1992).
[9] L. Tang, F. Wen, Y. Yang, C. T. Crowe, J. N. Chung, and T. R. Troutt, ''Self-organizing particle dispersion mechanism in a plane wake,'' Phys. Fluids A **4**, 2244 (1992).
[10] C. T. Crowe, T. R. Troutt, and J. N. Chung, ''Numerical models for two-phase turbulent flows,'' Annu. Rev. Fluid Mech. **28**, 11 (1996).
[11] G. R. Ruetsch and E. Meiburg, ''On the motion of small spherical bubbles in two-dimensional vortical flows,'' Phys. Fluids A **5**, 2326 (1993).
[12] K.-K. Tio, A. Liñán, and J. C. Lasheras, ''On the dynamics of buoyant and heavy particles in a periodic Stuart vortex flow,'' J. Fluid Mech. **254**, 671 (1993).
[13] G. R. Ruetsch and E. Meiburg, ''Two-way coupling in shear layers with dilute bubble concentrations,'' Phys. Fluids **6**, 2656 (1994).
[14] M. J. Manton, ''On the motion of a small particle in the atmosphere,'' Boundary Layer Meteorol. **6**, 487 (1974).
[15] F. A. Morrison, ''Inertial impaction in stagnation flow,'' Aerosol Sci. **5**, 241 (1973).
[16] B. V. Ramarao and C. Tien, ''Aerosol deposition in two-dimensional laminar stagnation flow,'' J. Aerosol Sci. **20**, 775 (1989).
[17] B. V. Ramarao and C. Tien, ''Role of Basset force on particle deposition in stagnation flow,'' J. Aerosol Sci. **21**, 597 (1990).
[18] M. R. Maxey and J. R. Riley, ''Equation of motion for a small rigid sphere in a non-uniform flow,'' Phys. Fluids **26**, 883 (1983).
[19] T. R. Auton, Ph.D. thesis, University of Cambridge, Cambridge, United Kingdom, 1981.
[20] R. Mei, C. J. Lawrence, and R. J. Adrian, ''Unsteady drag on a sphere with small fluctuations in the free-stream velocity,'' J. Fluid Mech. **233**, 613 (1991).

Downloaded¬22¬May¬2004¬to¬128.111.70.70.¬Redistribution¬subject¬to¬AIP¬license¬or¬copyright,¬see¬http://pof.aip.org/pof/copyright.jsp

[21]R. Mei, R. J. Adrian, and T. J. Hanratty, ''Particle dispersion in isotropic turbulence under Stokes drag and Basset force with gravitational setting,'' J. Fluid Mech. **225**, 481 (1991).
[22]R. Mei and R. J. Adrian, ''Flow past a sphere with an oscillation in the free-stream velocity and unsteady drag at finite Reynolds number,'' J. Fluid Mech. **237**, 323 (1992).
[23]R. Mei, ''Flow due to an oscillating sphere and an expression for the unsteady drag on the sphere at finite Reynolds number,'' J. Fluid Mech. **270**, 133 (1994).
[24]P. M. Lovalenti and J. F. Brady, ''The force on a sphere in a uniform flow with small-amplitude oscillations at finite Reynolds number,'' J. Fluid Mech. **256**, 607 (1993).
[25]P. M. Lovalenti and J. F. Brady, ''The force on a bubble, drop, or particle in arbitrary time-dependent motion at small Reynolds number,'' Phys. Fluids A **5**, 2104 (1993).
[26]P. M. Lovalenti and J. F. Brady, ''The hydrodynamic force on a rigid particle undergoing arbitrary time-dependent motion at small Reynolds number,'' J. Fluid Mech. **256**, 561 (1993).
[27]P. M. Lovalenti and J. F. Brady, ''The temporal behavior of the hydrodynamic force on a body in response to an abrupt change in velocity at small but finite Reynolds number,'' J. Fluid Mech. **293**, 35 (1995).
[28]E. J. Chang and M. Maxey, ''Unsteady flow about a sphere at low to moderate Reynolds number. Part 1. Oscillatory motion,'' J. Fluid Mech. **277**, 347 (1994).
[29]S. Elghobashi (personal communication, 1996).
[30]M. R. Maxey, ''The motion of small spherical particles in a cellular flow field,'' Phys. Fluids **30**, 1915 (1987).
[31]B. J. Lázaro and J. C. Lasheras, ''Particle dispersion in a turbulent, plane, free shear layer,'' Phys. Fluids A **1**, 1035 (1989).
[32]O. A. Druzhinin, ''Concentration waves and flow modification in a particle-laden circular vortex,'' Phys. Fluids **6**, 3276 (1994).
[33]M. J. Matsufuji and E. Hasegawa, ''Particle collision on the wall in a stagnation flow,'' Bull. J. Soc. Mech. Eng. **24**, 790 (1981).

Downloaded¬22¬May¬2004¬to¬128.111.70.70.¬Redistribution¬subject¬to¬AIP¬license¬or¬copyright,¬see¬http://pof.aip.org/pof/copyright.jsp